



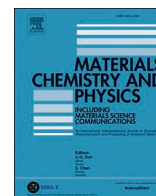
**University of
Sunderland**

Oladapo, Bankole, Kayode, Joseph, Karagiannidis, Panagiotis, Naveed, Nida, Ahmad Mehrabi, Hamid and Ogundipe, Kolawole (2022) Polymeric composites of cubic-octahedron and gyroid lattice for biomimetic dental implants. *Materials Chemistry and Physics*, 289. ISSN 0254-0584

Downloaded from: <http://sure.sunderland.ac.uk/id/eprint/14954/>

Usage guidelines

Please refer to the usage guidelines at <http://sure.sunderland.ac.uk/policies.html> or alternatively contact sure@sunderland.ac.uk.



Polymeric composites of cubic-octahedron and gyroid lattice for biomimetic dental implants

Bankole I. Oladapo^{a,b,*}, Joseph F. Kayode^c, Panagiotis Karagiannidis^a, Nida Naveed^a,
Hamid Mehrabi^a, Kolawole O. Ogundipe^d

^a School of Engineering, Faculty of Technology, University of Sunderland, UK

^b Sustainable Development, De Montfort University Leicester, UK

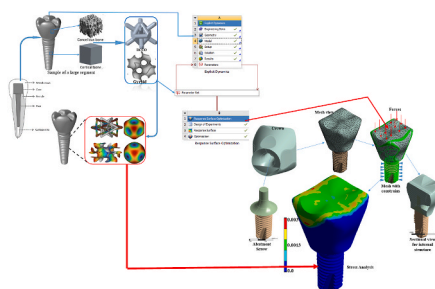
^c Department of Mechanical and Mechatronics Engineering, Afe Babalola University, Ado-Ekiti, Nigeria

^d Multisystem Hospital, Afe Babalola University, Ado-Ekiti, Nigeria

HIGHLIGHTS

- Designing and printing of variable macro-lattice structures of PEEK composite using FDM.
- Measure the compressive deformation behaviour of macro-lattice structures for dental implants.
- FEA helped us understand the behaviours of lattice structures of PEEK/cHAP in different ratios.
- Varying lattice designs of gyroid and BCCO can influence both strength and failure Implants.

GRAPHICAL ABSTRACT



ARTICLE INFO

Keywords:

3D printing
cHAP/PEEK
Composite scaffolds
Dental implants
Lattice structures

ABSTRACT

The study describes a homogenisation technique of developing a Polyether ether ketone (PEEK) and calcium hydroxyapatite (cHAP) composite with periodic pattern lattice structures. The continuum depiction of the discrete structures was evaluated to retain the PEEK cellulose composite properties of the lattice cell applied to dental implants. Design approaches were considered, using different software modelling to optimise the orthotropic lattice PEEK material by establishing an optimal variable cell lattice density distribution in the geometric model of a dental implant. A homogenising model was studied based on the lattice optimisation that resulted from the previous stage and considered different volume fractions, pore size, and variable density for different lattice cells for dental implants. Their adequate elastic fatigues were obtained by the unit cell's fast design-based model homogenisation method, and bioactivity cell tests took place in a culture medium. It was evident from the results obtained that the homogenisation increased the stiffness of the bracket by using the same cubic lattice cell, and the fundamental frequency obtained with lattice optimisation to higher results after implants. This result can easily be applied by using these lattice structures and PEEK composite in dental implants for medical industries and institutions as a lightweight and better biocompatible materials compared to metals.

* Corresponding author. School of Engineering, Faculty of Technology, University of Sunderland, UK.,
E-mail addresses: Bankole.Oladapo@research.sunderland.ac.uk, P17243433@my365.dmu.ac.uk (B.I. Oladapo).

<https://doi.org/10.1016/j.matchemphys.2022.126454>

Received 21 March 2022; Received in revised form 13 June 2022; Accepted 21 June 2022

Available online 30 June 2022

0254-0584/© 2022 The Authors. Published by Elsevier B.V. This is an open access article under the CC BY license (<http://creativecommons.org/licenses/by/4.0/>).

1. Introduction

The mechanical properties of materials are essential for practical use in the 3D printing of dental implants. When material development depends on changing the material composition to improve the material's mechanical properties, there is often a close relationship between the inherent properties of these materials, such as fatigue and density [1–3]. Polymer materials are manufactured structures whose mechanical properties can be manipulated by deformation and microstructure specifically for implants. Mechanical properties can be designed to have unique characteristics not found in nature, and lattice structures that mimic bone/dental structure arrangements can be considered. It depends on the microstructure and properties of the material from which it is made [4–6].

Polymers for dental implants generally have high fatigue and hardness, which have been studied extensively and deeply by many scientists. Different researchers [7–9] analysed the elastic properties of different theories of the lattice structure, like formula and beam lattice for an orthopaedic implant. These structures demonstrated the accurate deformation of the metamaterial with straight and curved lattice components standard in implants. They achieved an effective increase and variation in stiffness in a predefined direction along the direction of the lattice structure [10–12]. However, some studies have also found that local areas of high stress will cause severe structural damage. The structure exceeds the elastic limit due to material and microstructure restrictions. Therefore, it is necessary to find a way to strengthen the network structure—mesh made of materials subject to particularly severe damage and fatigue properties [13–15].

In recent years, tissue engineering structures have been designed using triple periodic minimum surfaces (TPMS) to overcome the geometric limitations of pore-forming elements, as TPMS exists in both natural and manufactured terms. Therefore, they are essential to scientists due to the concise description of various physical materials. Studies have established a primary cubic structure in a beam lattice and primitive using a layered production method [16,17]. These structures help create and ensure that propagation cells have access to blood and nutrients. TPMS scaffold design methodology was a means to accomplish this task. This program generated a gradient in pore size and porosity in computer-aided design (CAD) files showing known TPMS surface Designs under different software [18–20]. However, the cube-shaped samples created for display with random pore architecture resulting from leaching and static are not favourable to many bone implants.

On the other hand, an example of the experiment was the shape of the primary disk. Studies have recently described designing a computer-aided porous scaffold based on TPMS [21,22]. The work described a periodic surface TPMS that consists of simple trigonometric functions for mechanical, chemical, and physical applications. However, the selective agglutination of the powder is made by the action of a liquid adhesive at room temperature rather than a laser beam at high temperatures, as applicable to AM technology [23,24]. The selective release of the molten resin over the powder is done by a print head, the same as in inkjet printers for printing on paper. After being removed from the machine, the parts are cleaned of uncoated powder. Then, cyanoacrylate is infiltrated to provide mechanical reinforcement [25–27]. As the surface and dimension quality is lower than previously stated, AM is sometimes used as an instrument for visual or conceptual prototypes. These techniques can be used to produce scaffolds. The development of homogenisation methods for periodic media has also received substantial attention lately. Various strategies are used to get a continuum representation of the dynamic elastic behaviour of irregular domains while retaining information about their characteristics and geometry [28–30]. For wave propagation research, the emphasis has been on approximating the dynamic response of a regular system and dispersion relations. Multi-grid approaches based on asymptotic expansion, which have historically been used in classical homogenisation, have been suggested

[31,32]. For Eshelby's equivalent integration theory of self-consistency, general asymptotic homogenisation may be used to compute the effective characteristics, which can be done analytically or numerically. Recently, much attention has been paid to reducing the amount of tissue; for the most part, TPMS can distinguish biphasic substances into inter-related areas [33,34].

Hence, this work focuses on AM technology with designing gyroid and BCCO structures for dental implants with PEEK/cHAp composite materials. The method is relevant in tissue engineering for dental generation. The investigated applications of biomaterials as scaffolds for dental implants and utilising cells for creating artificial tissues were developed and analysed. A novel scaffold and design process were proposed to stimulate cellular growth, minimise artificial and cellular environments, and increase cellular differentiation, accelerating cell proliferation. This innovative study designed nearly isotropic hybrid cellular materials based on gyroid and BCCO surfaces. The elastic moduli of these cellular materials were confirmed on the unit cell, representing the implant's strength. Using the design-based model homogenisation method, all the elastic moduli of the lattices reached the upper bound of homogenisation simultaneously. This study also focused on 3D printing technology and morphological microanalysis for dental implant production in tissue engineering. Also, it used biological materials, like polymer materials and cHAp, for the scaffolding with different lattice cells to create artificial tissues. The design process and optimisation of lattice for dental implant with PEEK and composite (cHAp) with porous scaffold using homogenisation is shown in Fig. 1.

2. Materials and methods

An extruder by Filabot Triex LLC, USA, was utilised. It was fed consistently with 3×3 mm PEEK and cellulose composite fragments to obtain typical 3D-printed filaments with a diameter of 1.75 mm. The extruder temperature was set to about 350 °C, which is higher than the melting temperature of the cellulose composite, as determined by differential scanning calorimetry (DSC). Technology Outlet, the home of 3D printers, Leicestershire, UK deliver the PEEK materials. The filament released from the extruder nozzle was rolled around a roller following the AM method. Before the extrusion process, the extruder was purged carefully with pure PEEK [35–37]. The filaments were subsequently kept in a confined environment with low humidity and appropriate storage conditions, such as a low temperature, to prevent evaporation of the plasticisers. Being aware of the evaporation of the plasticisers over time, they were almost immediately used as a material source for the 3D printer [38–40]. The system included an extruder, thermal control, and traversing subsystems. The extruder subsystem was firmly installed on a rigid frame fixed to a granite plate.

2.1. FDM 3D printing settings for scaffold

A slight overlap allowed the walls to connect firmly to the infill, which is the pattern of the structure in the model. The infill was affected by the percentage infill, density, and pattern, which has an infill line distance of 0.4 mm with an infill thickness of 0.1 mm. The gradual infill steps are the number of times to reduce the infill density by half when getting further below the top surfaces set at zero [41,42]. Due to the solidification and cooling processes, the areas closer to the top surface of the scaffold got higher than the infill density. The layer thickness was always affected by layer height. The layer of infill materials was set at 0.1 mm. This value is always a multiple-layer height and is otherwise rounded up.

2.2. Design of lattices for femurs

The topological, joint, porous, pore-size, and available materials influence porous structures' mechanical and biological characteristics. Analysis was focused on four structural forms as archetype topology:

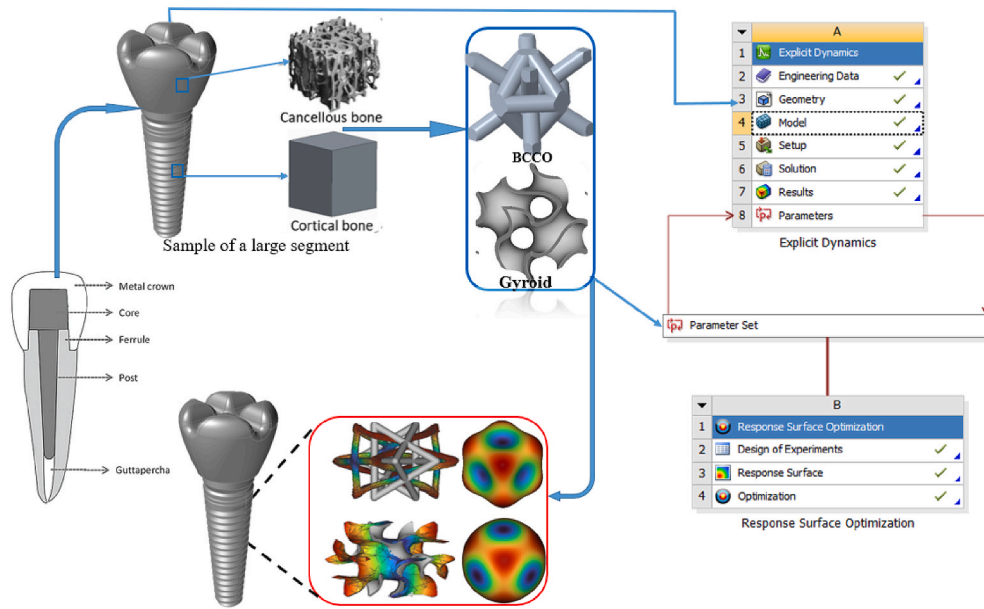


Fig. 1. The novel proposed designed lattice for dental implant with PEEK with porous scaffold using homogenisation.

gyroid and body centre cubic octahedron (BCCO), as illustrated in Fig. 2. The four structures possess high resistance to fracture and obtain design domains, and parametric geometric models were used. Furthermore, parametric modelling of each system was essential for establishing geometric parameters, porosity, and pore sizes. The percentage of space in a substantial cell was the same as in $P = 1 - V_p/V_s$ where volumes of the porous structure and system were expressed as V_p and V_s , respectively. Therefore, all the standard geometries of the structures provided a basis for the structure of the mechanical features necessary for the

structure design, using the geometric parameters, porosity, and pore sizes. Eqs (1)–(4) indicate the volumes of the four structures [43–45].

A single gyroid structure consists of iso-surfaces described by

$$\sin(x)\cos(y) + \sin(y)\cos(z) + \sin(z)\cos(x) > u(x, y, z), \quad (1)$$

Where the surface is constrained by $u(x, y, z)$.

$$V_{BCCO} = (3\pi/4) * D_o^2 a + 4\sqrt{3}\pi D_i^2 a / 4 - (3\pi/4) * D_o^3 - 4\sqrt{3}\pi D_i^3 / 4 \quad (2)$$

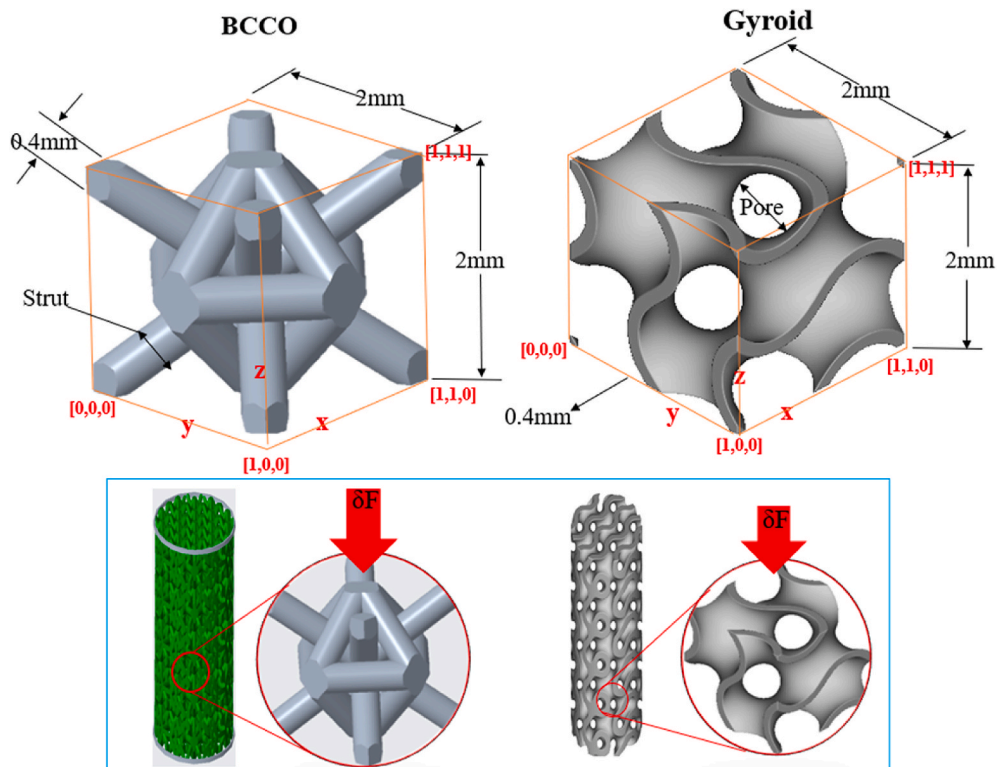


Fig. 2. These are examples of different proposed lattice CAD models for dental scaffold structures designed for this research utilised in model hybrid structure development.

Also, $V_s = a^3$

Pore sizes can be expressed from Eqs (1)–(3),

$$t_{BCCO} = a - D_o \tag{3}$$

Where t_i represents the thickness of the strut of different gyroid and BCCO structures, (v) denotes the volume of the cubic system and the size, respectively. The capability of 3D printing processing and dental growth conditions were restricted for structure design. The minimum pore dimensions of the medical scaffold were 300 μm , and N55% prepared the minimum strut thickness of 150 μm ; SLM technology has been used [46,47]. In the design of geometric structural parameters, these factors were considered.

2.3. Design analysis

The CAD body was created and then meshed by introducing implicit mesh convert from the CAD body in ntopology, which has a refinement level integration of maximum adaptive to allow (0, 9). Higher values improved the precision in the region where patches only approximate the limit of the Catmull-Clark surface. This region occurred around the one ring of an extraordinary vertex and along edges tagged semi-sharp. A surface mesh was introduced at an edge length of 0.1 on a triangle shape setting with a span angle of 30°, a growth rate of 2, and a feature angle of 45°. The mesh surface was sent into a split mesh for quality output mesh before being sent into the quadrangular mesh for further meshing. The CAD body created from the quadrangular mesh block allowed for an approximation of the Catmull-Clark subdivision surface as a collection of bicubic B-spline patches [40,48,49]. As the

quadrangular mesh dominant was given as the input up to two globals, Catmull-Clark refinement was performed to create a quad mesh represented by bicubic patches. This meshing was done because the final part failed to mesh appropriately due to the Parasolid body. A manifold mesh was introduced to the surface. When the quad mesh was introduced to the TPMS lattice cell structure, a quad count was captured for better curvature of the input mesh range of [0,1]. The sharp feature improved the auto-detection and preservation properties in the input mesh. The flow angle produced a minimum scalar value that defined the profile edge of the CAD body [38,50,51]. Fig. 3 shows the final production of the femur dental and the different TPMS lattice structures with an FDM 3D printer. The value that identified edges to preserve while remeshing the value represented a lower bound. The dihedral angle between the two faces was more significant than the criteria. The edge was tagged as a profile. This method was combined with preserving sharp edges, constraining the quad mesh's alignment to the profile edges, and giving the TPMS lattice model a symmetry plane.

$$\text{Modulus of Elasticity [E] is } \frac{\text{Stress}}{\text{Strain}} = \frac{\sigma}{\epsilon}, \text{ and} \tag{4}$$

Young Modulus (E)

$$E_c = E_p V_p + E_{cHAp} V_{cHAp} \tag{5}$$

shear modulus (G)

$$G_c = G_p V_p + G_{cHAp} V_{cHAp} \tag{6}$$

$$G_c = 1.375 \times 0.6 + 3.943 \times 0.4 = 2.4022$$

Density (ρ) kg/m³

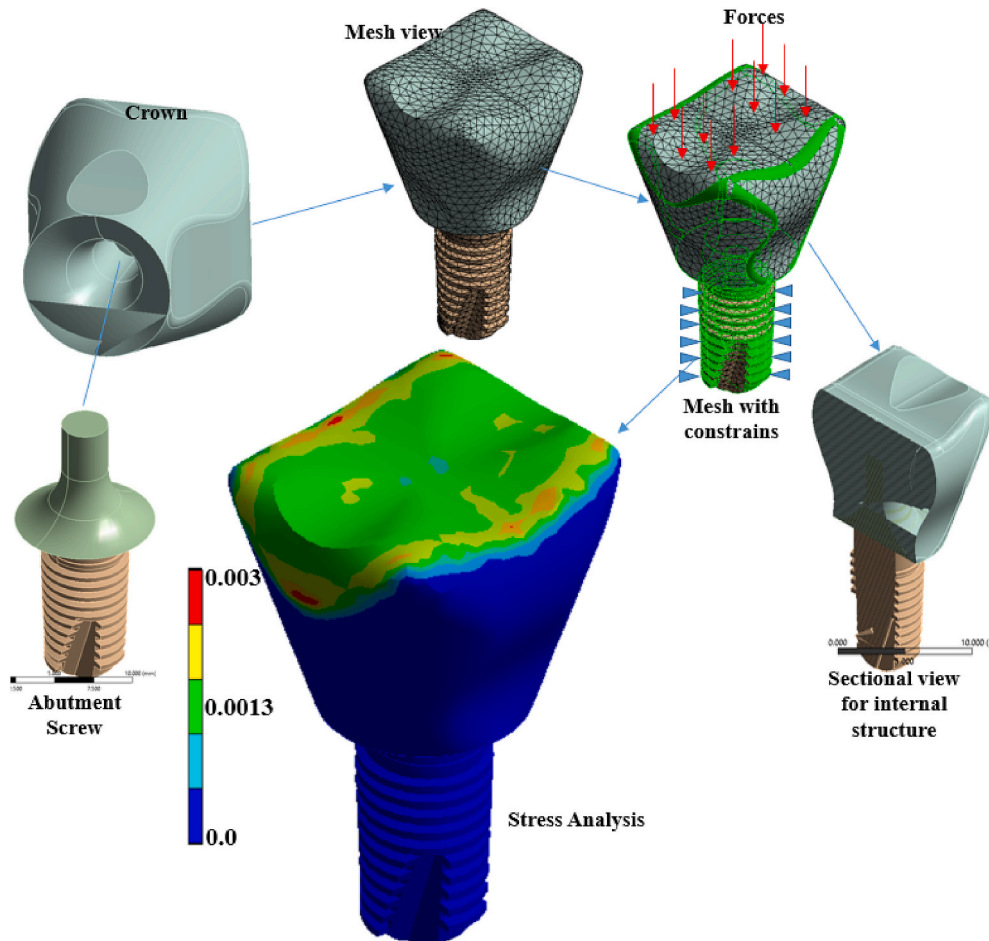


Fig. 3. Workflow and process of compressive test set-up and its analysis.

Table 1
Composite percentage weight of PEEK-cHAP of different densities at 1310 kg/m³ of PEEK density.

Sample	PEEK (wt%)	cHAP (wt%)	Young's modulus (E) Gpa	Shear Modulus (G) Gpa	Poisson Ratio (θ)	Density (ρ) kg/m ³	Bulk Modulus (Gpa)
PEEK	100	0.00	3.950	1.414	0.397	1310	6.392
PEEK 1	90.0	10.0	4.573	1.6318	0.4012	1503	7.715
PEEK 2	80.0	20.0	5.176	1.8886	0.3703	1686	6.653
PEEK 3	70.0	30.0	5.779	2.1454	0.3468	1869	6.288
PEEK 4	60.0	40.0	6.382	2.4022	0.3284	2052	6.197
Crown			8.2	3.154	0.3	2235	6.833

$$\dot{\rho}_c = \dot{\rho}_p V_p + \dot{\rho}_{cHAP} V_{cHAP} \quad (7)$$

$$\dot{\rho}_c = 1320 \times 0.6 + 3150 \times 0.4 = 2052$$

Therefore, the modulus of elasticity [E] values for the PEEK, and cHAP were 3.85 GPa, and 10 GPa respectively. The most used poison ratio (θ) for PEEK is 0.4, from which another composite poison ratio was derived. The density (ρ) of PEEK was 1310 kg/m³, and ρ of 3150 kg/m³ for cHAP. The modulus of rigidity or shear modulus (G) of PEEK and cHAP were 1.375 and 3.943 GPa, respectively, according to Eq. (4) (Table 1).

$$G = \frac{E}{2(1 - \theta)} \quad (8)$$

From Eq. (2), using 70 wt% of PEEK and 30 wt% of cHAP gives the expression:

$$E_c = 3.97\text{GPa} \times 0.6 + 10\text{GPa} \times 0.4$$

$$E_c = (2.382 + 4)\text{GPa} = 6.382\text{GPa}$$

$$E_c = 3.97\text{GPa} \times 0.7 + 10\text{GPa} \times 0.3$$

$$E_c = (2.779 + 3)\text{GPa} = 5.779\text{GPa}$$

$$E_c = 3.97\text{GPa} \times 0.8 + 10\text{GPa} \times 0.2$$

$$E_c = (3.176 + 2)\text{GPa} = 5.176\text{GPa}$$

$$E_c = 3.97\text{GPa} \times 0.9 + 10\text{GPa} \times 0.1$$

$$E_c = (3.573 + 1)\text{GPa} = 4.573\text{GPa}$$

2.4. Homogenizations analysis

The individual homogenisation of different cells in the cage was designed using Creo Parametric 7 and then analysed using the ntopology software. Homogeneous performances save computing time when designing dense truss structures. Homogeneous representation determined dense lattice structures in dental geometry without integrating the structural failure and confirmation model. Mathematical descriptions were stored and used in simulations to analyse the structural, linear, constant, and modal responses. A smaller model and quicker simulation were some benefits of this new approach to lattice optimisation. This difference was made because the homogenisation method can be used quickly on the noneconomic lattice [41,52,53].

In contrast, the general situation for the multi-atom lattice was more complex, and therefore, it was recommended here. Complementing a more superficial position and determining the appropriate boundary conditions can be a significant obstacle in developing a homogeneous formula and determining where to cut the Taylor series and the forecast order. The limited homogenisation command was used as the boundary condition applied load point. Boundary conditions and load consistency were avoided. The material's effective properties were extracted by homogenisation by fast Fourier transform (FFT). The significant advantages of this algorithm over traditional asymptomatic homogenisation include its higher efficiency, as it avoids finite element analysis

(FEA) over time. As its an autonomous method, the critical concepts can be summarised as follows: periodic cells were chosen to periodically study the linear elastic properties of the cellular material with its microstructural properties. Fig. 3 shows the 3D printing experimental process, the printing layers, and support for optimum FDM. Fig. 3 shows a variety of lattice CAD models for dental scaffold structures that could be used in this study [39,43].

3. Results and discussion

3.1. Lattice and homogenisation

Fig. 4 shows the fabrication of thin-bed geometry with unit cells and 2.0 × 2.0 × 2.0 strands compared with column-based trusses with joint and columnar architecture. These TPMS slabs were perfectly interconnected. Therefore, more materials can be used efficiently. Fig. 4 was the standard surface of the levelling function in a unit delimited by a lattice of 10 μm, which can neither be manipulated by asymptomatic calculation nor analysis homogenisation. They can be easily obtained with design-based model homogenisation in ntopology, a programme for simplicity. Generally, these members were equal to the units in the homogenisation process. The relative density in Fig. 4 ranged from 0.05 to 0.80, corresponding to the PEEK material with a similar geometric profile. However, it has different thicknesses. The efficiency values of cubic gyroid foam and octal lattice obtained by design-based model homogenisation were identical to FEA's. Moreover, Fig. 4 shows different 3D-printed cHAP and PEEK scaffolds of the structure design of gyroid and BCCO before and after adding cellulose composite to mimic dental structures, with 50p to show life representation and dimensions of the scaffolds. As a basis for evaluating the PEEK material of TPMS cells, cubic octal foam can approach the higher homogenisation bond of the higher bond than the TMPS cell material range maximum relative density. However, Neovius cell material performed better when $r > 0.4$ (Table 2).

3D printing allows parts with complex microstructures to be printed, sometimes using different scales. Using analysis of systems (ANSYS) Material Designer, the relationship between the associated length scales and the problem of the length scale difference when using a single finite element model can be significant. It presents a reduction in the size of the cell but enormous computational challenges. The standard approach in such cases is homogenisation. According to the scaling hypothesis, numerical homogenisation is often used to model cross-linked structures using comparable properties. Also, industrial support as a case study to analyse the effectiveness of homogenisation can be used. The hierarchical approach was developed and based on homogenisation to optimise the distribution and properties of materials, which has been critical in this context. Several studies [13,25,35,54] used numerical homogenisation to optimise the functional classification of the reticular structure. These studies used a single density variable to define the available isotropic lattice structures. Several methods have been developed to allow members of the different primary aspects of the cubic cell to vary in size independently [28,33,55]. These methods can make orthotropic trusses that can handle large-scale loads by letting cells in the unit move around. Fig. 5 shows the FEA of the deformation, elastic strain and von mises stress of pure PEEK. The corresponding composite shows the most

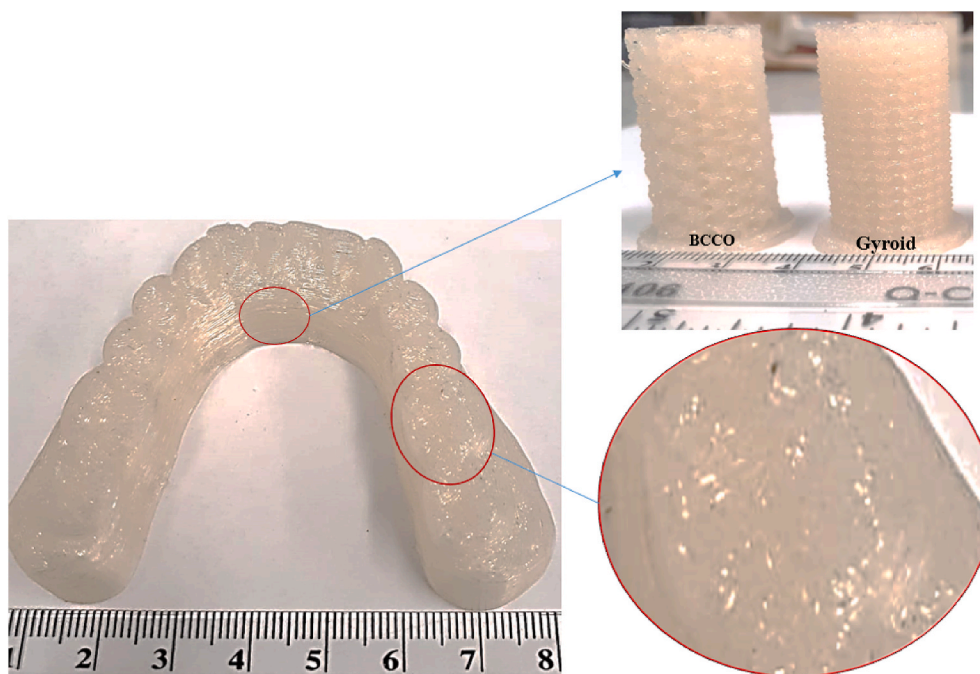


Fig. 4. Dental implant production and different TPMS lattice of gyroid and BCCO structures in FDM 3D printing.

Table 2

The composite combination of the three-part of the dental implant of the different composite and the corresponding result.

ABUTMENT	SCREW	CROWN	Elastic Strain	Stress [MPa]	Shear Stress [MPa]	Energy Total [mJ]	Deformation [mm]	Shear Elastic Strain
Ti-6Al-4V,	Ti-6Al-4V	Ti-6Al-4V	0.00166	166.2908	47.04528	38.97914	0.002002	0.001133
PEEK	PEEK	PEEK	0.003201	10.99508	3.795261	3.930727	0.002003	0.002685
PEEK 1	PEEK 1	PEEK 1	0.002986	12.4083	4.35256	4.368669	0.002	0.002667
PEEK 2	PEEK 2	PEEK 2	0.002976	13.93478	4.663437	4.258483	0.002003	0.002469
PEEK 3	PEEK 3	PEEK 3	0.002952	15.3932	5.007902	4.31436	0.002005	0.002334
PEEK 4	PEEK 4	PEEK 4	0.002915	16.76091	5.353133	4.421316	0.002003	0.002228
PEEK	PEEK 1	PEEK 2	0.002974	13.92436	4.659352	4.251946	0.002	0.002467
PEEK 1	PEEK 2	PEEK 3	0.00295	15.38254	5.003908	4.307976	0.002003	0.002332
PEEK 2	PEEK 3	PEEK 4	0.002917	16.77294	5.357593	4.428664	0.002005	0.00223
PEEK 3	PEEK 4	PEEK	0.003201	10.99248	3.794051	3.928782	0.002003	0.002684

stressful area of the dental implant. From Fig. 5 the von mises stress on the PEEK4 is more than the pure PEEK and another composite. It is seen that the increase in the quality of CHAp in the system increases the implant increase the stress it can withstand.

Fig. 5 FEA of a sectional view of the elastic deformation strain and von mises stress of 3 samples With the RVE modelling, the homogenisation process was initiated in ANSYS, which required creating simple geometry and determining the material properties of the components. Then, as stated in the present study, the geometry for FEA was carried out in a single step of complex computational pre-processing, leading to the produced material. It is homogeneous and has changeable characteristics, resulting in significantly lower macro simulation costs. The second strategy for the design of this study was to create a homogenised model that analysed the new model. The boundary conditions and nature of the finite element model were used in this study. The first modal analysis approach used type elements and dimensions. The non-optimised model was the main objective of the optimisation analysis. It was homogeneous and had changeable characteristics, producing significantly lower macro simulation costs.

Besides, Figs. 6 and 7 depict strength-level dental implant lattice structures with multiple cells of $2.0 \times 2.0 \times 2.0$ mm and the corresponding homogenisation within the range of Young's modulus of elasticity that mimic the dental structure. The first modal analysis approach used the terms type, element, and dimension. Similarly, it was homogeneous and had changeable characteristics, resulting in

significantly lower macro simulation costs. The second strategy for the design of this study was to create a homogenised model that analysed the new model. The boundary conditions and nature of the finite element model were used in this study and element and dimension in the first modal analysis approach. Fig. 6 Shows the top view of FEA of the model shear stress and strain of dental implant. From Fig. 6, there is more shearing effect on the pure PEEK and elastic expansion compared to the composite PEEK.

Finite elements with corresponding cubic cell sizes were $2.0 \times 2.0 \times 2.0$ mm. Topology optimisation was unsuccessful for smaller cell sizes. Interestingly, when the cell size decreased, the first two natural frequencies increased slightly for the homogenised model and were reduced somewhat for the following three times. Homogenisation for different cell topologies obtained the first six natural frequencies with a size of $\varnothing 20 \times 30$ mm³. Therefore, the modal analysis for the lattice structure was performed in two ways. The first approach was used to model the lattice structure obtained by the topological analysis. The second approach was used as a model. After optimising the cubic cell, the weight was reduced by more than half, from 45.50 to 21.77 kg. The cage and homogenisation gave equal mass values. It was assumed that the structure's geometry to be homogenised played a role in forming variable volume fractions, which varied the densities. The fundamental strength and fatigue were increased using the same cubic cell during the homogenisation process, which used various volume fractions that made up the orthotropic material.

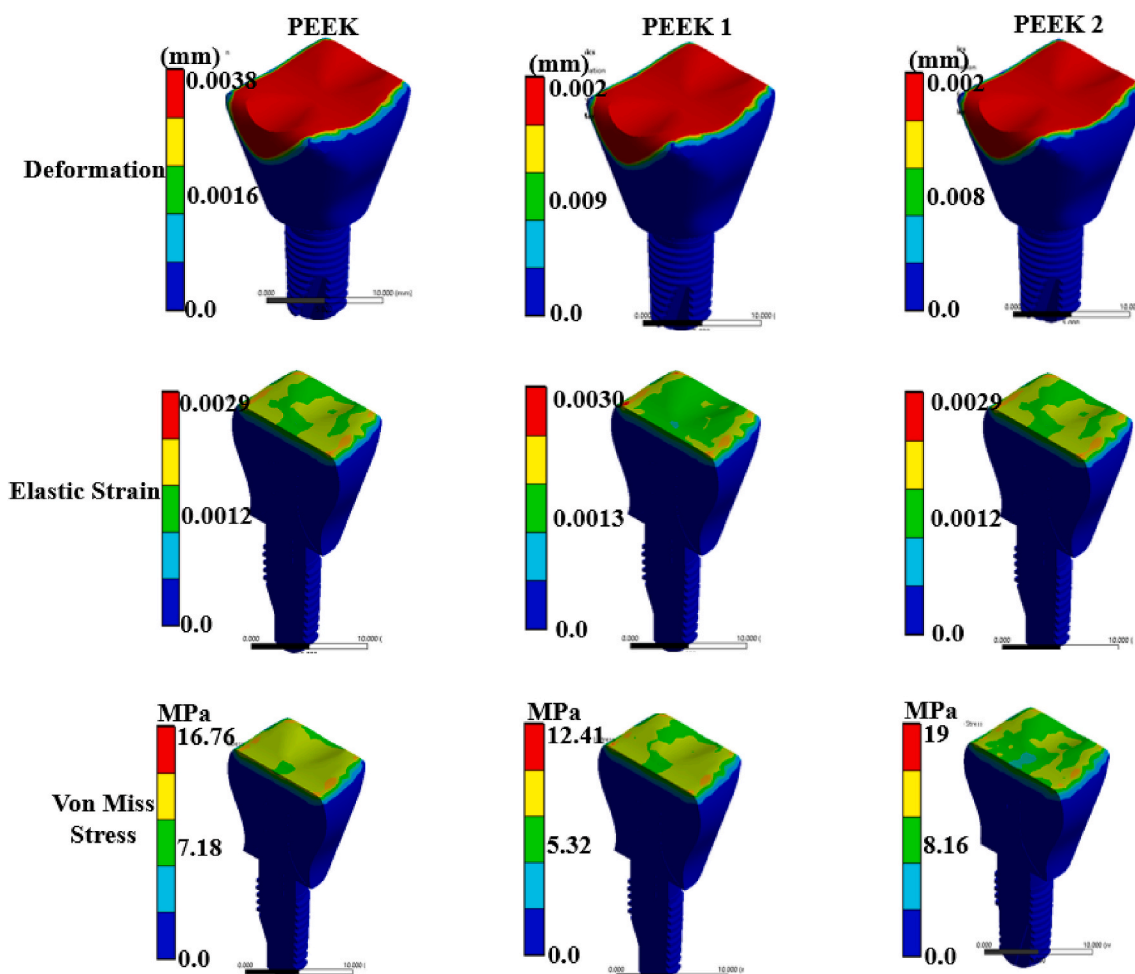


Fig. 5. The FEA of the deformation, elastic strain, and von mises stress of pure PEEK and corresponding composite showing the most stress area of the dental implant.

3.2. The lattice structure of cellulose composite and porosity

After 40 cycles, the cells maintained their intricate 3D lattice architectures, proving their mechanical strength and fatigue. As a result, a high volumetric capacity at low pressure can be achieved, which is necessary for bodily fluid transport. This breakthrough method is critical to the cell and medical device industries. The results showed that the research worked successfully with cell devices for biomedical applications, including miniaturised scaffolds. Microdevices and non-biological cells also helped this effort. The dental implant may also be effectively employed because of the batteries manufactured using this technology's low weight and large capacity. Lattice and gyroid structures of BCCO with 0.4 mm and two cells of 0.2 and 0.20 mm gyroid structures were constructed and analysed for their properties. SolidWorks was used to make a computer model of the porous structural design that was supposed to be there. Porosity was measured to ensure the computer model of porosity and the structure's shape were correct.

3.3. Comparison of experimental and FEA results

Fig. 7 (a)–(d) depict experimental and FEA results of the different lattice CAD models, showing the stress and strain graph behaviours of BCCO, and gyroid models, respectively. It was observed that both methods produced agreed outcomes, especially with PEEK and cellulose composites with lower percentages of cHAp. Accuracy of their results can be granted. Hence, the reliability and accurate predictability of the finite element models were established. Fig. 7. Show comparison of experimental and FEA results of the different lattice CAD models,

showing the stress and strain graph behaviours of a composite dental implant.

In addition, Fig. 8 compares experimental and FEA results of the different lattice CAD models of the dental implant of the PEEK and composite, showing strength over the samples of the unit cell. The scaffolds were compared with human dental of relative shear modulus versus cellulose composite relative density, as depicted in Fig. 8. It was evident that both Young's and shear moduli (strengths) of the cellulose composites increased with their percentage weights. These moduli were almost the same as human dental, especially at 4 wt% and above. Therefore, the cellulose composite scaffolds can be suitable alternatives for biomimetic heterogeneous artificial dental repair, as required in biomedical/dental tissue engineering.

4. Discussion

The graphics optimisation approach selects a new scaffold's optimal type and volumetric ratios. Scaffold type and volume ratio are the only variables presently used in the procedure that are adequate to show this concept. There are advantages in using optimisation methods. Designers benefit from this because it gives them a visual representation of the whole problem space. As a result, the selection criteria for the network and their influence on the response are well understood. A volume proportion of 0.49 of the six initially available scaffold types was superior to the worst-performing scaffold that satisfied the limits in the optimisation approach, resulting in the gyroid scaffold outperforming the others with a 10% increase in cell growth rate. An optimisation method that considers the minimal pore size limit of the scaffolds

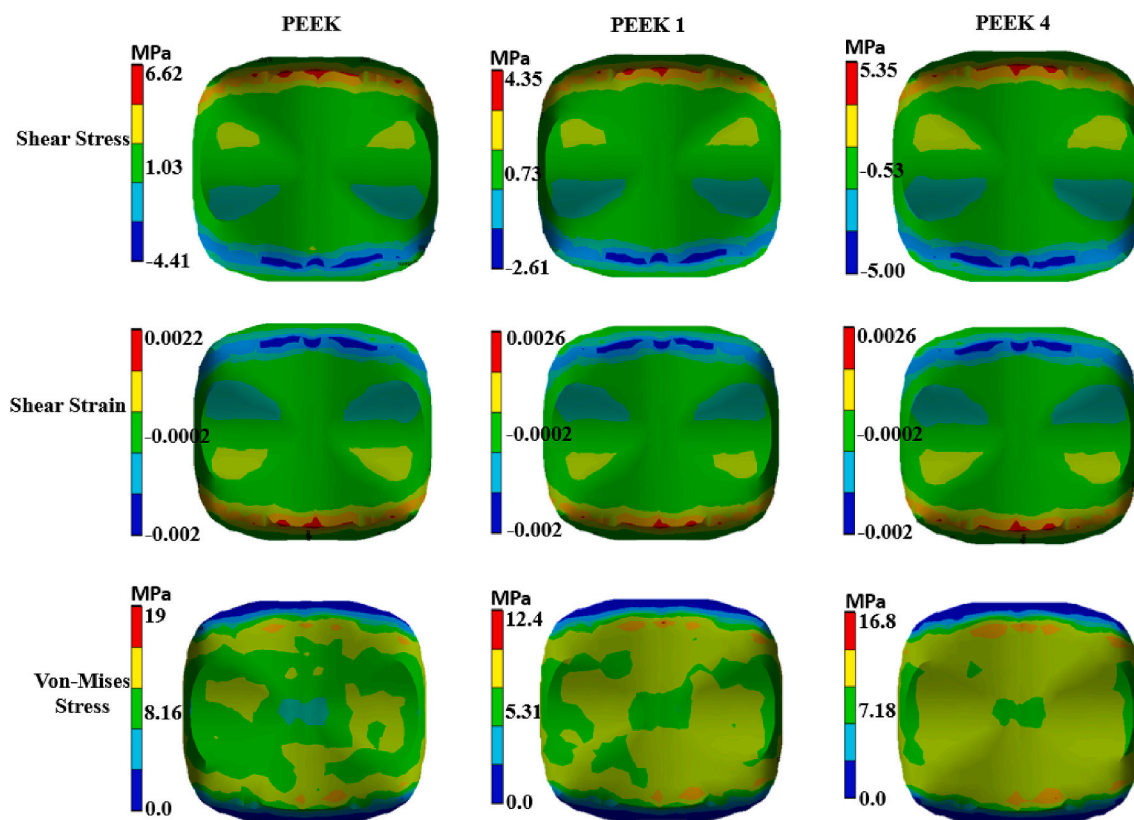


Fig. 6. The top view of FEA of the model shear stress and strain of dental implant.

induces capillaries to form across the network. The number of crossing spheres may be calculated using the suggested approach for determining the minimum pore size in a porous network.

Additionally, it is crucial to compute the top limit of the capillary pore size as a function of the diffusion of oxygen and nutrients. TPMS scaffolds can be compared accurately since they occupy the complete network of cells, making it easy to do so. Both capillaries are responsible for this outcome. The scaffold wall is too far away from the capillaries. The oxygen supply to the cells adhering to this wall is inadequate, and they perish. Mechanical stimulation of the skeleton and surrounding tissues influences dental development and growth outcomes. Stress may be beneficial. In gyroid cells, our findings demonstrate the importance of limiting rigidity. Allowable volume fractions are reduced by 74% with these restrictions.

Microscopic stratification models were used to simulate the growth of preosteoclast cells in TPMS structures. Ensemble-level models were previously validated with simpler geometries. As described in the method section, the practices used here differ from those in the original study. Although we have successfully revised our method, it showed an average cell growth rate [34–36]. It will continually decrease as the fractional amount increases. The gyroid scaffold type produces maximum cell growth for the optimal volume ratio and the range of all volume fractions. A recent study [33,56,57] shows the bioabsorbable scaffold model with visco-porous elastic dental. Although some numerical research has been done, this study does not suggest optimising the design parameters as we have done here. The gyroid and BCCO pattern is a cell pattern with excellent stable mechanical properties and good dental growth.

In particular, the mechanical performance of the gyroid and BCCO-designed scaffold was almost the same in all building orientations. Scaffolds made of gyroid and BCCO may be used in various orthopaedic procedures. It was worthwhile to investigate the gyroid and BCCO structure's failure mechanism in the event of a rise in voltage. Inner strut

deflection in the unit cell was predicted because of their propensity toward compression. A more significant number of investigations into the cellular structure are required. The dental structure cannot be adequately replicated in some instances due to a lack of cell structure. The discovery and creation of more arbitrary lattice structures are needed. It is essential to evaluate the practicality of creating a ramp. Additional ideas may be required for the overall and gradient structure designs. Considering the limits of AM technology is critical to success. Complex porous structures may be difficult to fabricate with AM technology. The design must consider the potential flaws of various printing methods. The porous structure's biological characteristics must be examined. In vitro and in vivo studies were compared to mechanical tests, particularly long-term in vivo tests.

Most structures on non-parametric engineering scaffolds are the same; they are all slight alterations to a straightforward construction. Microscopically, most cell architectures rely on cube-based structures while neglecting random and non-cube-based morphologies. Because of this, it is necessary to provide a comprehensive overview of the microstructure. TPMS and Voronoi scaffolds are now being developed at a rapid pace. Scaffolds with lattices that resemble porous dental performance have shown superior randomness. TPMS scaffolds have high permeability because of their smooth, continuous surface. Even with current research, is still much unknown and the design criteria and fatigue must be further investigated. To compare and assess various cell structures in orthopaedic and dental applications. The porous structure's minuscule components must be put through the same rigorous testing procedure.

5. Conclusions

The design-based model homogenisation approach was used to examine the mechanical characteristics of cellular materials with the ntopology of triply periodic minimal surfaces. Similar findings were

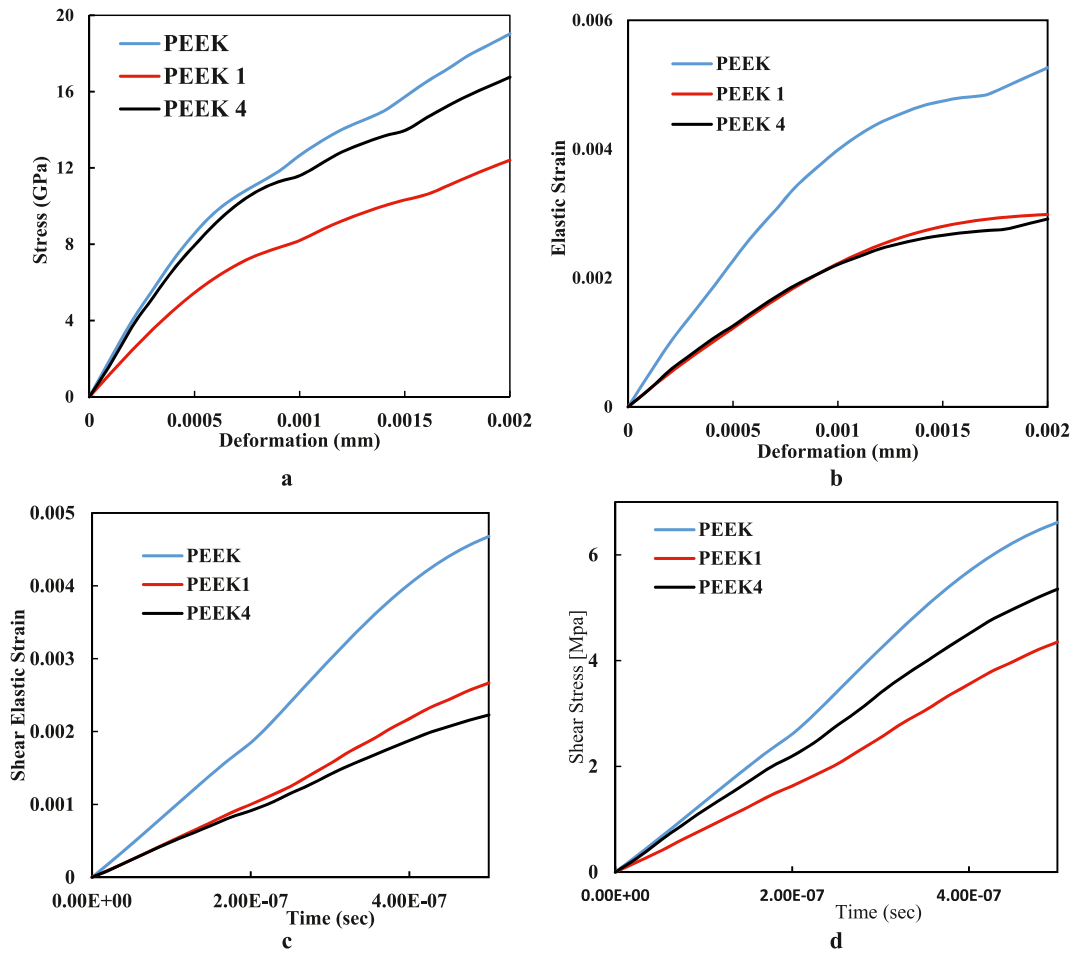


Fig. 7. Comparison of experimental and FEA results of the different lattice CAD models, showing the stress and strain graph behaviours of a composite of dental implant (a) Stress to deformation (b) Elastic strain to deformation (c) Shear Elastic strain to time of compression (d) Shear stress to the time.

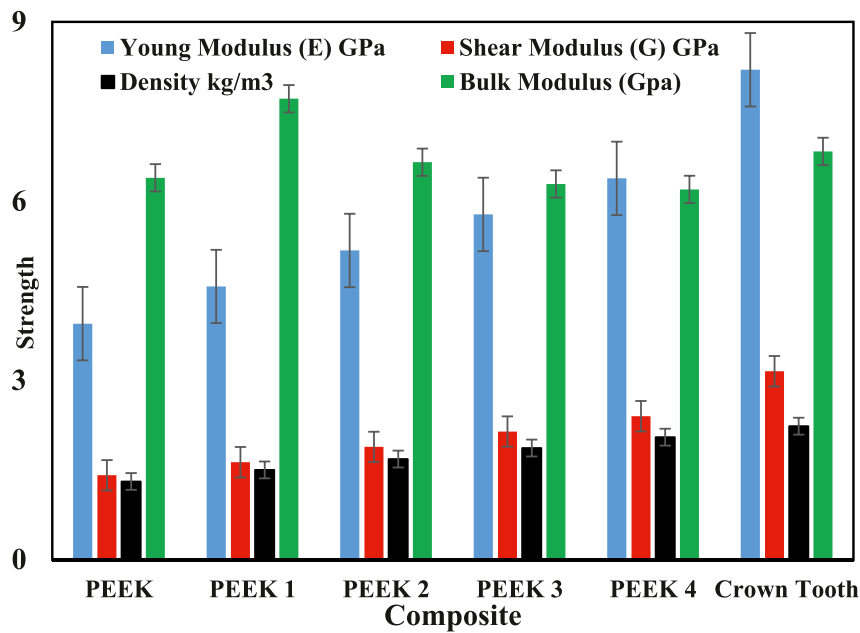


Fig. 8. Comparing compressive stress of the composite CAD models shows scaffolds compared with a human dental of relative strength versus cellulose composite of a dental implant sample.

easily obtained using the homogenisation technique for a lattice unit cell with elements measuring $2 \times 2 \times 2$ mm. As a result of this ground-breaking study, periodic lattice structures may be homogenised to aid biomedical engineering. FEA simulations changed the system's electrodynamic equation, then reversed and expanded using the Taylor series expansion. The proposed structural parameters can be applied to industrial design problems. Significantly, the proposed guidelines improved the precision of estimating the mechanical properties of extruded fibre materials. However, this method cannot guarantee the accuracy of the modified, graded, and paired lattice structures since the homogenisation procedures used in this investigation were determined over time. The limitation of homogenisation is that functionality works with square, cell-beam lattices that are uniformly distributed and require 3D printing of the entire geometry. Therefore, they are potential alternatives in dental tissue engineering. The tensile strength and Young's modulus of the cellulose composite containing 30 wt% and 40 wt% of cHAp, increased compared with the pure PEEK matrix. These demonstrated the value of uniformity for the mechanical features of the cellulose composites. Finally, the near-scope final impact of the lattice topology will be examined in future studies. Next, other mechanical properties, like interlayer resistance and deflection, will be studied with the help of the proposed approaches and the industrial design method.

Ethical statement

The authors declare no ethical issue; the study was conducted entirely with ethical standards. Also, the manuscript is neither under review nor published elsewhere.

Ethical approval

This study does not contain any studies with human or animal subjects performed by any authors.

Compliance with ethics guidelines

None.

CRediT authorship contribution statement

Bankole I. Oladapo: Conceptualization, Methodology, Software, Writing – original draft, Validation, Visualization, Investigation, Writing – review & editing, Funding acquisition, Resources. **Joseph F. Kayode:** Writing – review & editing, Investigation, Funding acquisition, Software, Project administration. **Panagiotis Karagiannidis:** Project administration, Validation, Writing – review & editing, Supervision, Writing – review & editing. **Nida Naveed:** Supervision, Writing – review & editing, acquisition, Visualization. **Hamid A. Mehrabi:** Supervision, Validation, Visualization, Writing – review & editing, acquisition.

Declaration of competing interest

The authors declare that they have no known competing for financial interests or personal relationships that could have appeared to influence the work reported in this paper.

Acknowledgement

None.

References

- [1] A.A. Stepashkin, D.I. Chukov, F.S. Senatov, A.I. Salimon, A.M. Korsunsky, S. D. Kaloshkin, 3D-printed PEEK-carbon fiber (CF) composites: structure and thermal properties, *Compos. Sci. Technol.* 164 (2018) 319–326, <https://doi.org/10.1016/j.compscitech.2018.05.032>.
- [2] B.I. Oladapo, S.A. Zahedi, S.O. Ismail, F.T. Omigbodun, 3D printing of PEEK and its composite to increase biointerfaces as a biomedical material- A review, *Colloids Surf. B Biointerfaces* 203 (2021), 111726, <https://doi.org/10.1016/j.colsurfb.2021.111726>.
- [3] B.I. Oladapo, A.V. Adebiyi, E.I. Elemure, Microstructural 4D printing investigation of ultra-sonication biocomposite polymer, *J. King Saud Univ.-Eng. Sci.* 33 (2021) 54–60.
- [4] A. Dawood, B. Marti Marti, V. Sauret-Jackson, A. Darwood, 3D printing in dentistry, *Br. Dent. J.* 219 (2015) 521–529, <https://doi.org/10.1038/sj.bdj.2015.914>.
- [5] A.M. Wazeh, M.I. El-Anwar, R.M.G. Atia, R.M. Mahjari, S.A. Linga, L.M.A. Al-Pakistani, et al., 3D FEA study on implant threading role on selection of implant and crown materials, *Open Access Maced. J. Med. Sci.* 6 (2018) 1702–1706, <https://doi.org/10.3889/oamjms.2018.331>.
- [6] B.I. Oladapo, S.A. Zahedi, A.O.M. Adeoye, 3D printing of bone scaffolds with hybrid biomaterials, *Compos. B Eng.* 158 (2019) 428–436, <https://doi.org/10.1016/j.compositesb.2018.09.065>.
- [7] B.I. Oladapo, S.A. Zahedi, S.O. Ismail, F.T. Omigbodun, O.K. Bowoto, M. A. Olawumi, et al., 3D printing of PEEK-cHAp scaffold for medical bone implant, *Bio-Des. Manuf.* 4 (2021) 44–59, <https://doi.org/10.1007/s42242-020-00098-0>.
- [8] G. Aranovich, P. Donohue, M. Donohue, A lattice model for fluids with directional interactions, *J. Chem. Phys.* 111 (1999) 2050–2059, <https://doi.org/10.1063/1.479473>.
- [9] B.I. Oladapo, O.B. Obisesan, B. Oluwole, V.A. Adebiyi, H. Usman, A. Khan, Mechanical characterisation of a polymeric scaffold for bone implant, *J. Mater. Sci.* 55 (2020) 9057–9069.
- [10] T. Albrektsson, T. Jemt, J. Mölne, P. Tengvall, A. Wennerberg, Institute of Clinical Sciences D of B, et al., On inflammation-immunological balance theory—a critical apprehension of disease concepts around implants: mucositis and marginal bone loss may represent normal conditions and not necessarily a state of disease, *Clin. Implant Dent. Relat. Res.* 21 (2019) 183–189, <https://doi.org/10.1111/cid.12711>.
- [11] I. Buj-Corral, A. Tejo-Otero, F. Fenollosa-Artés, Development of AM technologies for metals in the sector of medical implants, *Baseline* 10 (2020) 686, <https://doi.org/10.3390/met10050686>.
- [12] O.K. Bowoto, B.I. Oladapo, S.A. Zahedi, F.T. Omigbodun, O.P. Emenuvwe, Analytical modelling of in situ layer-wise defect detection in 3D-printed parts: additive manufacturing, *Int. J. Adv. Manuf. Technol.* 111 (2020) 2311–2321.
- [13] B.I. Oladapo, E.A. Oshin, A.M. Olawumi, Nanostructural computation of 4D printing carboxymethylcellulose (CMC) composite, *Nano-Struct. Nano-Object.* 21 (2020), 100423.
- [14] F. Alam, K.M. Varadarajan, J.H. Koo, B.L. Wardle, S. Kumar, Additively manufactured polyetheretherketone (PEEK) with carbon nanostructure reinforcement for biomedical structural applications, *Adv. Eng. Mater.* 22 (2020), 2000483, <https://doi.org/10.1002/adem.202000483> n/a.
- [15] M. Nasr Azadani, A. Zahedi, O.K. Bowoto, B.I. Oladapo, A review of current challenges and prospects of magnesium and its alloy for bone implant applications, *Prog. Biomater.* (2022) 1–26.
- [16] M. Braun, J. Aranda-Ruiz, J. Fernández-Sáez, Mixed mode crack propagation in polymers using a discrete lattice method, *Polymers* 13 (2021) 1290, <https://doi.org/10.3390/polym13081290>.
- [17] A. Du Plessis, I. Yadroitsava, I. Yadroitsev, S. Roux, D. Blaine, Numerical comparison of lattice unit cell designs for medical implants by additive manufacturing, *Virtual Phys. Prototyp.* 13 (2018) 1–16, <https://doi.org/10.1080/17452759.2018.1491713>.
- [18] J. Feng, B. Liu, Z. Lin, J. Fu, Isotropic octet-truss lattice structure design and anisotropy control strategies for implant application, *Mater. Des.* 203 (2021), 109595, <https://doi.org/10.1016/j.matdes.2021.109595>.
- [19] D. Mahmoud, M.A. Elbestawi, Lattice structures and functionally graded materials applications in additive manufacturing of orthopedic implants: a review, *J. Manuf. Mater. Process.* 1 (2017) 13, <https://doi.org/10.3390/jmmp1020013>.
- [20] B.I. Oladapo, S.O. Ismail, O.M. Ikumapayi, J.F. Kayode, Impact of rGO-coated PEEK and lattice on bone implant, *Colloids Surf. B Biointerfaces* (2022), 112583.
- [21] D. Ali, M. Ozalp, S.B. Blanquer, S. Onel, Permeability and fluid flow-induced wall shear stress in bone scaffolds with TPMS and lattice architectures: a CFD analysis, *Eur. J. Mech.-B/Fluids* 79 (2020) 376–385.
- [22] C. Yan, L. Hao, A. Hussein, P. Young, Ti-6Al-4V triply periodic minimal surface structures for bone implants fabricated via selective laser melting, *J. Mech. Behav. Biomed. Mater.* 51 (2015) 61–73.
- [23] J. Zhang, Y. Shen, Y. Sun, J. Yang, Y. Gong, K. Wang, et al., Design and mechanical testing of porous lattice structure with independent adjustment of pore size and porosity for bone implant, *J. Mater. Res. Technol.* 18 (2022) 3240–3255.
- [24] B.I. Oladapo, S.O. Ismail, A.V. Adebiyi, F.T. Omigbodun, M.A. Olawumi, D. B. Olawade, Nanostructural interface and strength of polymer composite scaffolds applied to intervertebral bone, *Colloids Surf. A Physicochem. Eng. Asp.* 627 (2021), <https://doi.org/10.1016/j.colsurfa.2021.127190>.
- [25] X. Guo, X. Zheng, Y. Yang, X. Yang, Y. Yi, Mechanical behavior of TPMS-based scaffolds: a comparison between minimal surfaces and their lattice structures, *SN Appl. Sci.* 1 (2019) 1–11.
- [26] O. Al-Ketan, D.-W. Lee, R. Rowshan, R.K.A. Al-Rub, Functionally graded and multi-morphology sheet TPMS lattices: design, manufacturing, and mechanical properties, *J. Mech. Behav. Biomed. Mater.* 102 (2020), 103520.
- [27] J. Ge, J. Huang, Y. Lei, P. O'Reilly, M. Ahmed, C. Zhang, et al., Microstructural features and compressive properties of SLM Ti6Al4V lattice structures, *Surf. Coat. Technol.* 403 (2020), 126419.

- [28] L. Yang, Y. Li, S. Wu, P. Chen, H. Wu, J. Su, et al., Tailorable and predictable mechanical responses of additive manufactured TPMS lattices with graded structures, *Mater. Sci. Eng., A* 843 (2022), 143109.
- [29] N. Strömberg, Optimal grading of TPMS-based lattice structures with transversely isotropic elastic bulk properties, *Eng. Optim.* 53 (2021) 1871–1883.
- [30] B.I. Oladapo, S.A. Zahedi, F.T. Omigbodun, A systematic review of polymer composite in biomedical engineering, *Eur. Polym. J.* 154 (2021), 110534, <https://doi.org/10.1016/j.eurpolymj.2021.110534>.
- [31] C. Chatzigeorgiou, B. Piotrowski, Y. Chemisky, P. Laheurte, F. Meraghni, Numerical investigation of the effective mechanical properties and local stress distributions of TPMS-based and strut-based lattices for biomedical applications, *J. Mech. Behav. Biomed. Mater.* 126 (2022), 105025.
- [32] B.I. Oladapo, V. Balogun, Electrical energy demand modeling of 3D printing technology for sustainable manufacture, *Int. J. Eng.* 29 (2016) 954–961.
- [33] A. Karakoç, RegionTPMS — region based triply periodic minimal surfaces (TPMS) for 3-D printed multiphase bone scaffolds with exact porosity values, *SoftwareX* 16 (2021), 100835, <https://doi.org/10.1016/j.softx.2021.100835>.
- [34] S. Yu, J. Sun, J. Bai, Investigation of functionally graded TPMS structures fabricated by additive manufacturing, *Mater. Des.* 182 (2019), 108021, <https://doi.org/10.1016/j.matdes.2019.108021>.
- [35] S. Ma, Q. Tang, X. Han, Q. Feng, J. Song, R. Setchi, et al., Manufacturability, mechanical properties, mass-transport properties and biocompatibility of triply periodic minimal surface (TPMS) porous scaffolds fabricated by selective laser melting, *Mater. Des.* 195 (2020), 109034, <https://doi.org/10.1016/j.matdes.2020.109034>.
- [36] K.B. Sagomonyants, M.L. Jarman-Smith, J.N. Devine, M.S. Aronow, G. A. Gronowicz, The in vitro response of human osteoblasts to polyetheretherketone (PEEK) substrates compared to commercially pure titanium, *Biomaterials* 29 (2008) 1563–1572, <https://doi.org/10.1016/j.biomaterials.2007.12.001>.
- [37] B.I. Oladapo, S.A. Zahedi, Improving bioactivity and strength of PEEK composite polymer for bone application, *Mater. Chem. Phys.* 266 (2021), 124485.
- [38] B.I. Oladapo, I.A. Daniyan, O.M. Ikumapayi, O.B. Malachi, I.O. Malachi, Microanalysis of hybrid characterisation of PLA/CHA polymer scaffolds for bone regeneration, *Polym. Test.* 83 (2020), 106341, <https://doi.org/10.1016/j.polymertesting.2020.106341>.
- [39] B.I. Oladapo, S.A. Zahedi, S.O. Ismail, Mechanical performances of hip implant design and fabrication with PEEK composite, *Polymer* 227 (16) (2021), 123865, <https://doi.org/10.1016/j.polymer.2021.123865>. In this issue.
- [40] B.I. Oladapo, S.O. Ismail, O.K. Bowoto, F.T. Omigbodun, M.A. Olawumi, M. A. Muhammad, Lattice design and 3D-printing of PEEK with Ca10(OH)(PO4)3 and in-vitro bio-composite for bone implant, *Int. J. Biol. Macromol.* 165 (2020) 50–62, <https://doi.org/10.1016/j.ijbiomac.2020.09.175>.
- [41] B.I. Oladapo, S.A. Zahedi, S.O. Ismail, D.B. Olawade, Recent advances in biopolymeric composite materials: future sustainability of bone-implant, *Renew. Sustain. Energy Rev.* 150 (2021), 111505, <https://doi.org/10.1016/j.rser.2021.111505>.
- [42] O.P. Bodunde, O.M. Ikumapayi, E.T. Akinlabi, B.I. Oladapo, A.O. Adeoye, S. O. Fatoba, A futuristic insight into a "nano-doctor": a clinical review on medical diagnosis and devices using nanotechnology, *Mater. Today Proc.* 44 (2021) 1144–1153.
- [43] B.I. Oladapo, A.O.M. Adeoye, M. Ismail, Analytical optimisation of a nanoparticle of microstructural fused deposition of resins for additive manufacturing, *Compos. B Eng.* 150 (2018) 248–254, <https://doi.org/10.1016/j.compositesb.2018.05.041>.
- [44] B.I. Oladapo, S.O. Ismail, M. Zahedi, A. Khan, H. Usman, 3D printing and morphological characterisation of polymeric composite scaffolds, *Eng. Struct.* 216 (2020), 110752, <https://doi.org/10.1016/j.engstruct.2020.110752>.
- [45] B.I. Oladapo, S.A. Zahedi, S.O. Ismail, Assessing 3D printing of Poly (ether-etherketone) and cellular cHAp to increase biointerfaces as a biomedical material, *Colloids Surf. B Biointerfaces* (2021), 111726.
- [46] M.M. Costa, T.A. Dantas, F. Bartolomeu, N. Alves, F.S. Silva, G. Miranda, et al., Corrosion behaviour of PEEK or β -TCP-impregnated Ti6Al4V SLM structures targeting biomedical applications, *Trans. Nonferrous Met. Soc. China* 29 (2019) 2523–2533, [https://doi.org/10.1016/S1003-6326\(19\)65160-5](https://doi.org/10.1016/S1003-6326(19)65160-5).
- [47] I. Volyanski, S. Volchkov, I. Shishkovsky, Cytotoxicity and apoptotic effects of polymer coated copper oxide nanoparticles synthesised via SLM in mesenchymal stem cells, *Opt. Quant. Electron.* 49 (2017) 1–10, <https://doi.org/10.1007/s11082-017-0957-z>.
- [48] I.O. Bankole, S. Aban, M.T. Azeze, S.O. Afolabi, Computer aided drafting and construction of standard drafting table for college of engineering studio in afe babalola university, *Comput. Aided Draft Constr. Stand. Draft Table Coll. Eng. Studio AFE BABALOLA Univ.* 6 (2015) 1–8.
- [49] B.I. Oladapo, B.A. Vincent, A.O. Oke, E.A. Agbor, Design and finite element analysis on car seat height screw adjuster using autodesk inventor, *Int. J. Sci. Res. Environ. Sci.* 2 (2015).
- [50] C.O. Ijagbemi, B.I. Oladapo, H.M. Campbell, C.O. Ijagbemi, Design and simulation of fatigue analysis for a vehicle suspension system (VSS) and its effect on global warming, *Procedia Eng.* 159 (2016) 124–132.
- [51] Oladapo BI, Zahedi SA, Balogun VA, Ismail SO, Samad YA. Overview of Additive Manufacturing Biopolymer Composites 2021.
- [52] B.I. Oladapo, S.A. Zahedi, F. Vahidnia, O.M. Ikumapayi, M.U. Farooq, Three-dimensional finite element analysis of a porcelain crowned tooth, *Beni-Suef. Univ. J. Basic Appl. Sci.* 7 (2018) 461–464.
- [53] B.I. Oladapo, S.O. Ismail, T.D. Afolalu, D.B. Olawade, M. Zahedi, Review on 3D printing: fight against COVID-19, *Mater. Chem. Phys.* 258 (2021), 123943.
- [54] A.B. Olorunsola, O.M. Ikumapayi, B.I. Oladapo, A.O. Alimi, A.O. Adeoye, Temporal variation of exposure from radio-frequency electromagnetic fields around mobile communication base stations, *Sci. Afr.* 12 (2021), e00724, <https://doi.org/10.1016/j.sciaf.2021.e00724>. In this issue.
- [55] M. Fantini, M. Curto, F. De Crescenzo, TPMS for interactive modelling of trabecular scaffolds for bone tissue engineering, *Adv. Mech. Des. Eng. Manuf.* (2017) 425–435. Springer.
- [56] D. Mahmoud, M.A. Elbestawi, Selective laser melting of porosity graded lattice structures for bone implants, *Int. J. Adv. Manuf. Technol.* 100 (2019) 2915–2927, <https://doi.org/10.1007/s00170-018-2886-9>.
- [57] L. He, X. Liu, C. Rudd, Additive-manufactured gyroid scaffolds of magnesium oxide, phosphate glass fiber and polylactic acid composite for bone tissue engineering, *Polymers* 13 (2021) 270, <https://doi.org/10.3390/polym13020270>.